

OPEN

Arsenite exposure suppresses adipogenesis, mitochondrial biogenesis and thermogenesis via autophagy inhibition in brown adipose tissue

Jiyoung Bae^{1,2}, Yura Jang^{1,3}, Heejeong Kim¹, Kalika Mahato¹, Cameron Schaecher^{1,4}, Isaac M. Kim¹, Eunju Kim⁵ & Seung-Hyun Ro¹ 

Arsenite, a trivalent form of arsenic, is an element that occurs naturally in the environment. Humans are exposed to high dose of arsenite through consuming arsenite-contaminated drinking water and food, and the arsenite can accumulate in the human tissues. Arsenite induces oxidative stress, which is linked to metabolic disorders such as obesity and diabetes. Brown adipocytes dissipating energy as heat have emerging roles for obesity treatment and prevention. Therefore, understanding the pathophysiological role of brown adipocytes can provide effective strategies delineating the link between arsenite exposure and metabolic disorders. Our study revealed that arsenite significantly reduced differentiation of murine brown adipocytes and mitochondrial biogenesis and respiration, leading to attenuated thermogenesis via decreasing UCP1 expression. Oral administration of arsenite in mice resulted in heavy accumulation in brown adipose tissue and suppression of lipogenesis, mitochondrial biogenesis and thermogenesis. Mechanistically, arsenite exposure significantly inhibited autophagy necessary for homeostasis of brown adipose tissue through suppression of Sestrin2 and ULK1. These results clearly confirm the emerging mechanisms underlying the implications of arsenite exposure in metabolic disorders.

Obesity is a significant risk factor for several prevalent diseases, such as diabetes, hypertension, cardiovascular diseases, and cancers^{1–4}. White adipose tissue (WAT) and brown adipose tissue (BAT) are the main types of adipose tissue in humans⁵. In contrast to WAT's functions for energy storage, BAT is specialized to produce ATP through enriched intracellular mitochondria and heat through non-shivering thermogenesis via the uncoupling protein 1 (UCP1)^{6–9}. UCP1 proteins are localized in the inner membrane of brown adipocyte mitochondria to uncouple ATP synthesis from respiration^{10–13}. While BAT quickly regresses following birth^{5,14}, new evidence has revealed symmetrical fat depots in adults that have classic BAT features^{15–18}. Therefore, BAT has become a novel target for obesity treatment and prevention.

Arsenite, a most potent trivalent form of arsenic, is presented in water, soil, and foods due to its abundance in earth crust and the use of arsenite-contaminated pesticides and insecticides¹⁹. Arsenite is accumulated in various tissues and organs including adipose tissues, lung, heart, kidney, brain, eye, liver, hair, bone, and spleen^{20–22}. Thus, arsenite contaminated drinking water has been considered as a contributing factor for numerous health concerns in humans such as diabetes, lung and skin diseases, and cancer^{23–25}. Recent evidence suggests that exposure to arsenite may lead to adipose tissue dysfunction and lipodystrophy as well as inhibition of adipogenesis^{26,27}. Arsenite inhibits adipogenesis and adipocyte function in human mesenchymal stem cells²⁸, 3T3-L1 preadipocytes²⁹, and C3H 10T1/2 preadipocytes³⁰. The mechanisms underlying adipose tissue dysfunction and inhibition

¹Department of Biochemistry, University of Nebraska, Lincoln, NE, 68588, USA. ²Department of Cell and Regenerative Biology, University of Wisconsin School of Medicine and Public Health, Madison, WI, 53705, USA. ³Department of Neurology, The Johns Hopkins University School of Medicine, Baltimore, MD, 21205, USA. ⁴College of Medicine, University of Nebraska Medical Center, Omaha, NE, 68198, USA. ⁵Department of Mechanical and Materials Engineering, University of Nebraska, Lincoln, NE, 68588, USA. Jiyoung Bae, Yura Jang and Heejeong Kim contributed equally. Correspondence and requests for materials should be addressed to S.-H.R. (email: shro@unl.edu)

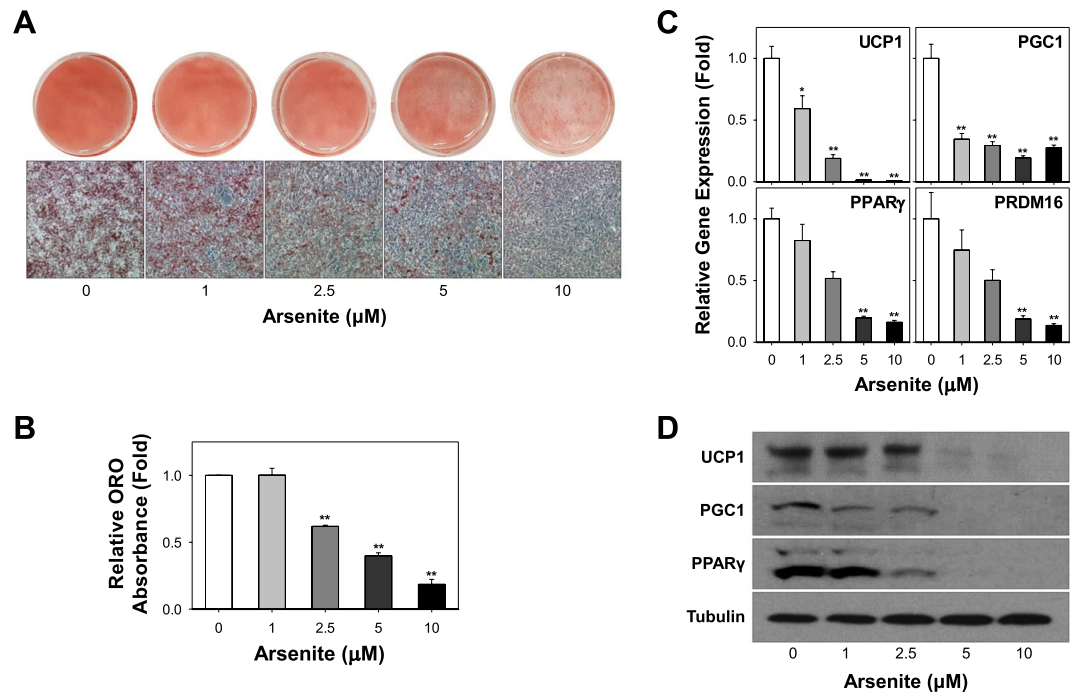


Figure 1. Arsenite exposure suppresses differentiation of HIB1B brown preadipocytes. (A) HIB1B brown preadipocytes were differentiated in the presence of increasing doses of arsenite (1–10 μM) or the vehicle control. (B) Oil Red O (ORO) staining was performed for cell morphology and ORO absorbance at Day 6 (D6) was measured. (C, D) After the differentiation of brown preadipocytes in the presence of increasing doses of Arsenite (1–10 μM) at Day 6, mRNA and protein expression of established brown markers were analyzed by qRT-PCR (C) and immunoblotting (D), respectively. At least 9 independent experiments were performed and all data was expressed as mean ± SEM. * $P < 0.05$ or ** $P < 0.01$ by One-way ANOVA analysis.

of adipogenesis by arsenite have been the focus of intense research. Recent studies suggest that arsenite-induced lipolysis is mediated through transcriptional factors, including peroxisome proliferator-activated receptor-gamma (PPAR γ) and CCAAT-enhancer binding protein alpha (C/EBP α)^{28,29}, as well as β -adrenergic receptor signaling³¹.

Autophagy is a delicate cellular recycling process in response to environmental and genotoxic stresses, which digests damaged proteins and organelles as a defense mechanism³². Mechanistically known so far, AMPK positively regulates autophagy induction through phosphorylating and activating ULK1, mammalian homologue of autophagy kinase Atg1, at Ser317, Ser555, and Ser777 whereas mTORC1 inhibits autophagy induction through phosphorylating and inhibiting ULK1 at Ser757^{33–36}. ULK1 regulates downstream autophagosomal receptors and autophagosomal maturation proteins such as p62³⁷ and LC3B, a mammalian homologue of autophagy-related gene (Atg) 8³⁸. Recent studies have shown that autophagy plays an important role in 3T3-L1 adipogenesis and lipid metabolism. Autophagy deficient 3T3-L1 preadipocytes block differentiation into mature adipocytes³⁹. Moreover, Atg5 or Atg7 deficient primary mouse embryonic fibroblasts (MEF) impair adipogenesis, and autophagy inhibitor, such as bafilomycin A1 and chloroquine, blocks primary MEF differentiation^{40,41}.

Despite arsenite-induced defect in adipogenesis and fat accumulation in WAT, the roles of arsenite in regulating the functions of BAT remain to be elucidated. Here, we report the impacts of arsenite exposure on the functions and activities of brown adipocytes and BAT. In cultured brown adipocytes, arsenite treatment reduced adipogenesis, mitochondrial biogenesis, respiration and thermogenesis. Arsenite exposure in live mice resulted in heavy arsenic accumulation in BAT but not in WAT. Accumulated arsenite suppressed lipogenesis, mitochondrial biogenesis and thermogenesis in BAT. Autophagy activity was significantly reduced by arsenite exposure through inhibition of Sestrin2 and ULK1. Our data provides the novel mechanisms underlying the effects of arsenite exposure on the physiological functions of BAT and reveals the significance of autophagy in protection against arsenite-induced damage in BAT.

Results

Arsenite suppresses HIB1B brown adipocyte differentiation. To investigate the effects of arsenite on brown adipocyte differentiation, immortalized HIB1B brown preadipocytes were differentiated in the presence of various doses of arsenite (1–10 μM) or the vehicle control. Arsenite dose-dependently suppressed brown adipocyte lipid accumulation, as revealed by Oil Red O stained multiocular, lipid-filled brown adipocytes (Fig. 1A). 10 μM of arsenite treatment decreased brown adipocyte differentiation up to 82% (Fig. 1B). Up to 10 μM of arsenite did not affect cell viability confirmed by MTT assays for up to 6 days (Fig. S1). mRNA expression of brown adipocyte specific markers, uncoupling protein 1 (UCP1), peroxisome proliferator-activated receptor-gamma coactivator 1 (PGC1), peroxisome proliferator activator receptor gamma (PPAR γ), and PR domain containing 16 (PRDM16) ($P < 0.01$) was significantly decreased by arsenite treatment (Fig. 1C). Attenuated protein expression

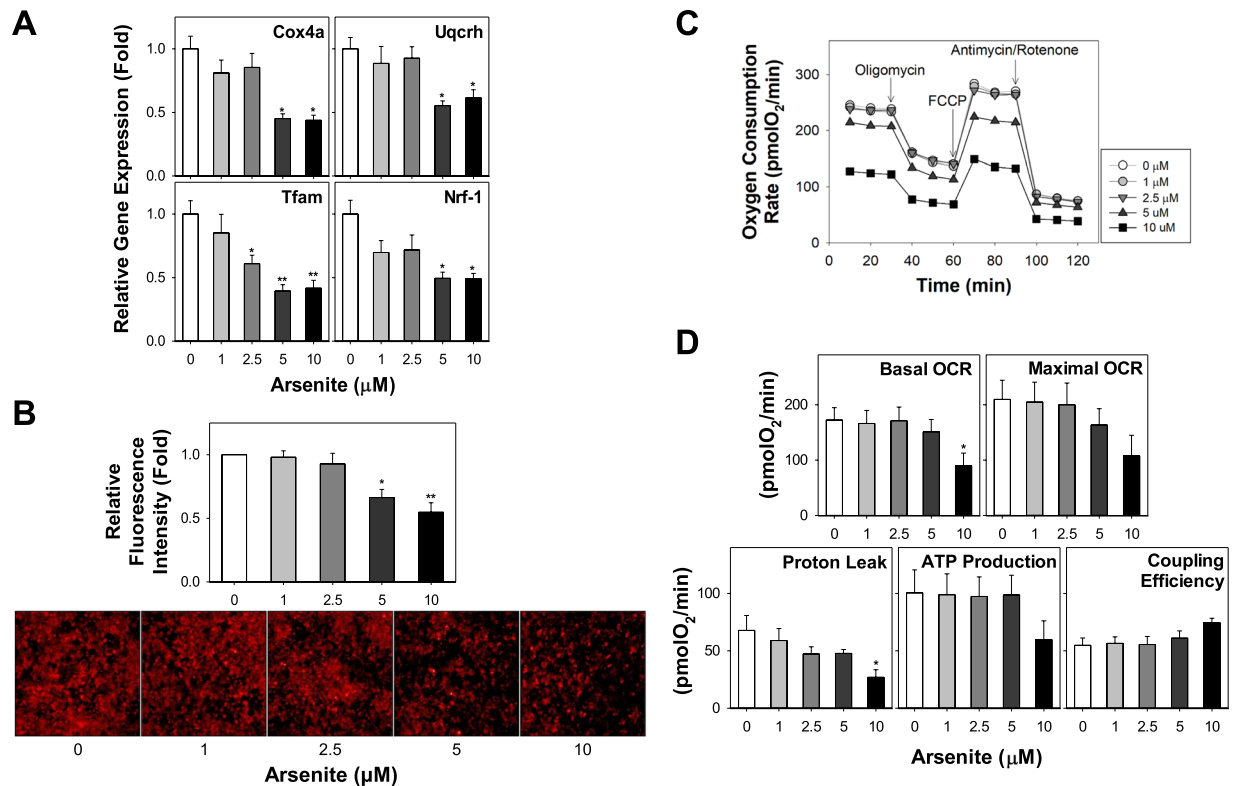


Figure 2. Arsenite dose-dependently suppresses mitochondria-associated marker genes, content and mitochondrial respiration in brown adipocytes. (A) Brown preadipocytes were differentiated in the presence of increasing doses of arsenite (1–10 μM) or the vehicle control. mRNA expression of mitochondrial structural genes, *Cox4a*, and *Uqcrrh*, and transcriptional factors, *Tfam* and *Nrf-1*, at Day 6 (D6) was measured. (B) Mitochondrial content was analyzed by mitochondrial-specific fluorescence dye MitoTracker at Day 6. Relative fluorescence intensity was calculated from the mean fluorescence intensity values of the samples and expressed as fold of the control. (C) Brown preadipocytes were seeded in 24-well XF assay plates and differentiated in the presence of increasing doses of arsenite (1–10 μM) or the vehicle control until Day 6. The cells were subjected to real-time measurements of oxygen consumption rate. At least 9 independent experiments were performed and all data was expressed as mean \pm SEM. * $P < 0.05$ or ** $P < 0.01$ by One-way ANOVA analysis.

of UCP1, PGC1, and PPAR γ (Fig. 1D) was consistent with decreased mRNA expression levels, suggesting that arsenite negatively affect differentiation of HIB1B brown preadipocytes by downregulating expression levels of essential brown adipocyte specific markers in both gene and protein.

Arsenite suppresses mitochondrial biogenesis and respiration in HIB1B brown adipocytes.

Analysis of mRNA expression showed that arsenite also suppressed mRNA levels of nucleus-encoded mitochondrial genes, cytochrome c oxidase subunit IV a (*Cox4a*) and cytochrome b-c1 complex subunit 6 (*Uqcrrh*), and transcription factors regulating mitochondrial gene expression, transcription factor A (*Tfam*) and nuclear respiratory factor 1 (*Nrf-1*) (Fig. 2A). Consistent with the mRNA expression results, mitochondrial biogenesis demonstrated by the staining of mitochondrial specific fluorescence MitoTracker Red was also decreased by arsenite treatment (Fig. 2B). To determine whether the suppression of mitochondria biogenesis by arsenite leads to decrease in mitochondrial uncoupling and thermogenesis, we examined oxygen consumption rates coupled with mitochondrial stress tests in brown adipocytes which have been differentiated in the presence or absence of arsenite by cellular bioenergetics measurements using XF24 Extracellular Flux Analyzers. Arsenite at 10 μM significantly decreased basal oxygen consumption rate (OCR) and proton leak; however, arsenite did not affect the maximal OCR, ATP production, and coupling efficiency (Fig. 2C,D).

Autophagy activity was inhibited by arsenite treatment during brown adipocyte differentiation.

We examined whether autophagy signaling underlies brown adipocyte differentiation, immunoblotting analysis showed that autophagy activity was up-regulated during brown adipocyte differentiation consistent with previous report in 3T3-L1 white adipocyte differentiation⁴². Autophagosome marker, microtubule-associated protein 1 light chain 3-II (LC3B-II, mammalian homologue of Atg8) and autophagosome substrate p62 (aka sequestosome 1) were both degraded by active autophagolysosome upto 50% by 10 μM arsenite treatment, phosphorylation of unc-51 like autophagy activating kinase 1 (ULK1) at Ser 555, which is AMPK target site, was increased and phosphorylation of ribosomal protein S6 kinase (S6K) at Thr 389, which is mTORC1 target site, was

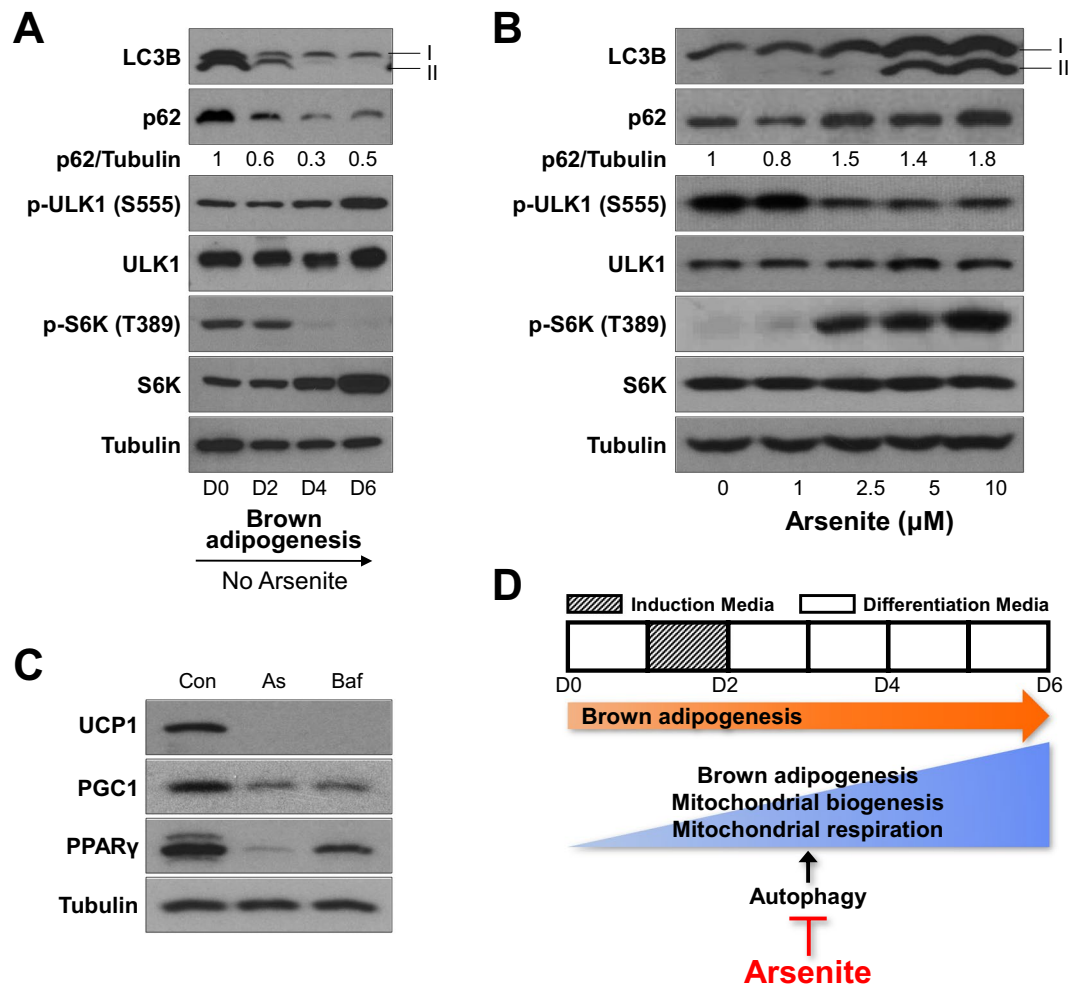


Figure 3. Arsenite inhibits autophagy which is necessary during brown adipocytes differentiation. (A) HIB1B brown adipocytes were differentiated without arsenite treatment and whole cell lysates at Day 0, 2, 4, and 6 (D0, 2, 4, and 6) were analyzed for autophagy activity. (B) Brown preadipocytes were differentiated in the presence of increasing doses of arsenite (1–10 μM) or the vehicle control until Day 6 (D6). Whole cell lysate was prepared and analyzed by immunoblotting with specific antibodies. (C) Arsenite (10 μM), Bafilomycin A1 (0.1 μM) or the vehicle control was treated during the differentiation of brown adipocytes and the protein levels of differentiation markers were measured by immunoblotting. (D) Schematic diagram depicting the toxic effect of arsenite on brown adipogenesis via inhibition of mitochondria function, thermogenesis and autophagy. At least 9 independent experiments were performed.

decreased upon brown adipocyte differentiation process (Fig. 3A). We also confirmed that arsenite suppressed autophagy induction during brown adipocytes differentiation revealed by accumulation of both LC3B-II and p62 upto 1.6 times in 10 μM of arsenite, decrease of ULK1 activity (p-Ser 555) and increase of S6K phosphorylation (p-Thr 389) when the cells were treated with arsenite in dose dependent manner (Fig. 3B). We examined the effect of the autophagy inhibitor, bafilomycin A1, on expression of brown adipocyte specific markers. Bafilomycin A1 significantly attenuated the expression of UCP1, PGC1, and PPAR γ protein expression levels in brown adipocytes (Fig. 3C), suggesting that autophagy pathway is necessary for brown adipogenesis, and supporting our hypothesis that arsenite suppresses brown adipocyte differentiation and function via autophagy inhibition through ULK1 inhibition and mTORC1 activation (Fig. 3D).

Arsenite was heavily accumulated in brown adipose tissue of mice after oral administration.

Knowing that arsenite treatment suppresses the differentiation and mitochondrial function of mouse brown adipocytes in dose dependent manner (Figs 1 and 2), we investigated whether arsenite can be accumulated on mouse BAT in physiological condition. First, the arsenic accumulation was quantified in mouse BAT and WAT using the inductively coupled plasma mass spectrometry (ICP-MS) after administration of arsenite by oral gavage at doses of 5 and 10 mg/kg once a day for 9 days (Fig. 4A,B). The control group was given water at the same volume of arsenite treatment groups. The relative amount of arsenite in BAT and WAT of those mice was compared. The concentration of arsenic accumulated in BAT was 4.5 times and 7.9 times higher than that in WAT ($P < 0.01$) in mice that were treated with 5 mg/kg and 10 mg/kg treatment groups, respectively.

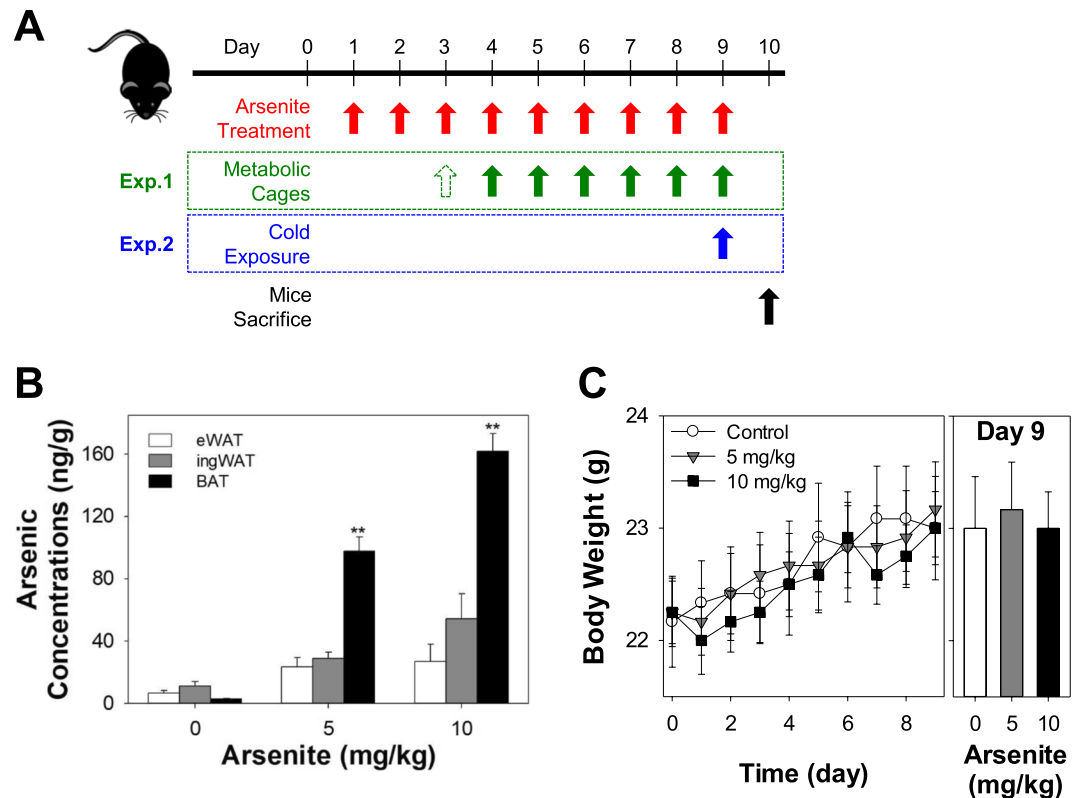


Figure 4. Arsenite is heavily accumulated in brown adipose tissue (BAT) but not in white adipose tissue (WAT) of mice. **(A)** Experimental design for mouse work. **(B)** The arsenic accumulation was quantified in eWAT, ingWAT, and BAT of C57BL/6 mouse using ICP-MS after the oral administration of arsenite at doses of 0 (control), 5, and 10 mg/kg/day for 9 days ($n=6$). Adipose tissues of all mice were collected on Day 10 under anesthesia with isoflurane and CO_2 . **(C)** Measurement of body weights ($n=12$). All data was expressed as mean \pm SEM. * $P < 0.05$ or ** $P < 0.01$ by One-way ANOVA analysis.

Although previous report identified that arsenic can majorly be accumulated in liver, kidney, and lung^{19,25}, we never expected such a high and differential accumulation between BAT and WAT in mice. Given that the accumulated concentration of arsenic in BAT but not in WAT was increased in dose-dependent manner, we anticipated that some of physiological parameters of mouse would be affected by arsenite accumulation in BAT. However, we could not observe any significant differences in body weight (Fig. 4C) and food and water intakes (Fig. S2A) between control and arsenite treatment groups. We also did not observe any significant differences in oxygen consumption (VO_2) and respiratory exchange ratio (RER, VO_2/VCO_2) when normalized by mouse body weight (Fig. S2B,C).

Arsenite down regulates the gene expression of brown adipose markers *in vivo*. To evaluate the effects of accumulated arsenite on BAT homeostasis in mice, we measured mRNA expression of brown adipose specific markers, UCP1, PGC1, PPAR γ , and PRDM16, after the oral administration of arsenite at doses of 5 and 10 mg/kg/day for 9 days (Fig. 5A). Lipogenic gene, PGC1 and PPAR γ , expression levels of 10 mg/kg group were significantly down regulated compared to those of control group ($P < 0.05$). The mRNA expression of nucleus-encoded mitochondrial biogenesis genes, Cox4a, Uqcrh, Tfam, and Nrf-1, were also measured on mice BAT (Fig. 5B). Uqcrh and Nrf-1 gene expression levels of 10 mg/kg group were significantly decreased compared to those of control group ($P < 0.01$). These data suggest that arsenite accumulated in 10 mg/kg group effectively suppresses brown adipocyte function and mitochondrial biogenesis. A well-known function of BAT is non-shivering thermogenesis that has been spotlighted in the regulation of obesity pandemic^{43,44}. Since UCP1 expression is augmented when exposed to cold in BAT of mice⁴⁵, we hypothesized that UCP1 inhibition by arsenite would be more dramatic and significant because UCP1 is further induced under by cold exposure. To investigate the effects of arsenite on UCP1 expression in non-shivering thermogenesis in mouse BAT, we challenged the mice in cold condition (4°C) for 24 hrs at the last day of arsenite administration (Fig. 4A). Arsenite administration (10 mg/kg) significantly reduced UCP1 ($P < 0.01$) and PPAR γ ($P < 0.05$) gene expression levels while there was no significant difference in PGC1 and PRDM16 gene expression levels (Fig. 5A). In the case of genes involved in mitochondrial biogenesis, Tfam and Nrf-1 gene expression levels of 10 mg/kg group were significantly reduced compared to those of control group ($P < 0.05$) whereas Cox4a and Uqcrh had no significant difference (Fig. 5B). Consistent with the gene expression level of UCP1, protein expression level of UCP1 was also suppressed by arsenite exposure in cold condition in mice BAT (Fig. 5C). Combined together, these data suggest that arsenite (10 mg/kg for 9 days) may suppress

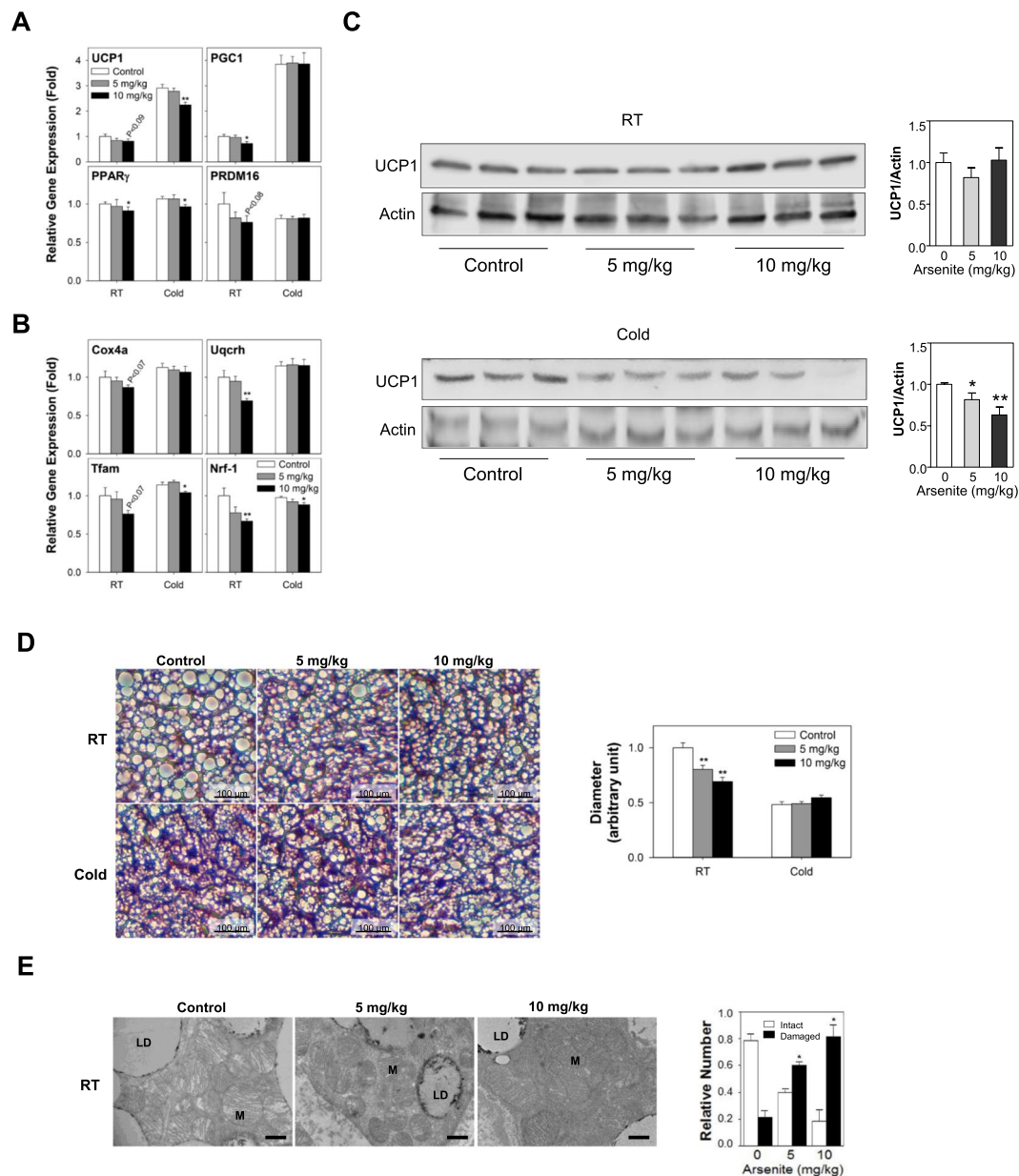


Figure 5. Arsenite down regulates the gene expression of brown adipocyte markers including thermogenesis gene UCP1 of mouse BAT *in vivo*. (A,B) mRNA expression levels of BAT markers (A) and mitochondrial biogenesis genes (B) were analyzed by qRT-PCR after the oral administration of arsenite into mice at doses of 0 (control), 5, and 10 mg/kg/day for 9 days. Mice were challenged with room temp (RT, 23 °C) control or cold temp (Cold, 4 °C) for 24 hrs on the last day of oral gavage to evaluate thermogenesis function ($n = 6$). (C) Protein expression level of UCP1 from mice BAT after administered with 0 (control), 5, and 10 mg/kg/day arsenite for 9 days (RT) and exposed to cold temp for 24 hrs before euthanization was analyzed by immunoblotting ($n = 3$). Relative band intensities were quantified through densitometry (ImageJ, NIH). (D) H&E staining of mouse BAT after arsenite administration and quantitative analysis of lipid droplet size ($n = 6$). Black scale bars represent 100 μm . (E) TEM image of mouse BAT after arsenite administration and quantitative analysis of relative number of intact and damaged mitochondria ($n = 3$). LD, lipid droplet, M, mitochondria. Scale bar, 800 nm. All data was expressed as mean \pm SEM. * $P < 0.05$ or ** $P < 0.01$ by One-way ANOVA analysis.

thermogenesis through the inhibition of UCP1 expression. Consistent with the suppression of adipogenesis genes such as PGC1 and PPAR γ , arsenite decreased the lipid droplet (LD) diameter of BAT in mice at room temperature (23 °C). However, in the BAT of mice exposed to cold (4 °C) for 24 hrs at the last day of arsenite administration, LD diameter was not significantly changed regardless of arsenite doses (Fig. 5D) possibly due to no significant change in PGC1 and PRDM16. Nevertheless, the overall reduction of lipid content under cold temperature relative to room temperature would reflect the induction in thermogenesis by activating UCP1 in

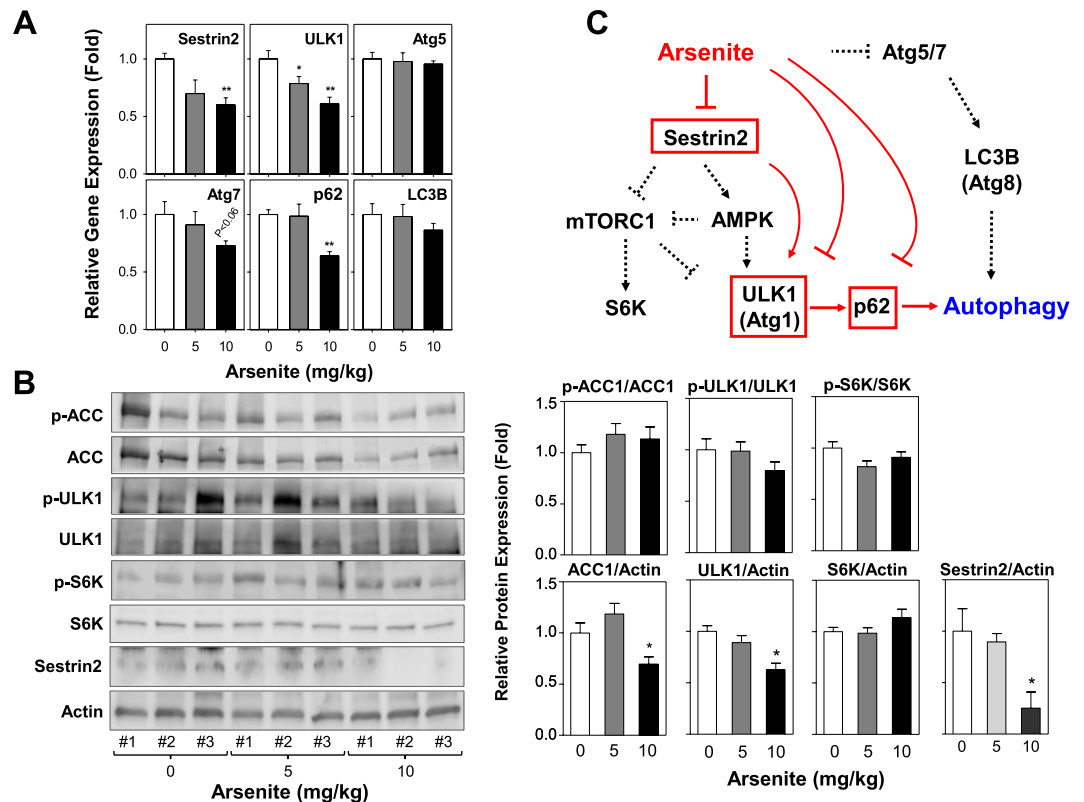


Figure 6. Arsenite inhibits autophagy in mouse BAT. (A) mRNA expression levels of autophagy genes in mouse BAT were analyzed after the oral administration of arsenite into mice at doses of 0 (control), 5, and 10 mg/kg/day for 9 days. (B) Protein expression levels of autophagy pathway genes were measured by immunoblotting in mouse BAT ($n = 3$) after arsenite administration. Relative phosphorylation band intensities were quantified through densitometry (ImageJ, NIH) and presented as mean \pm SEM ($n = 3$). * $P < 0.05$ by One-way ANOVA analysis. (C) Proposed model of how arsenite suppresses autophagy activity in BAT. Arsenite administration suppresses autophagy mainly through direct inhibition of Sestrin2 and ULK1. Arsenite suppresses gene expressions of p62 so that autophagosome receptor binding is blocked in mouse BAT. Arsenite has no significant effect on Atg5- or Atg7-dependent autophagosome conjugation system.

BAT. The UCP1 inhibition by arsenite could not be enough to observe a significant increase in LD diameter. Transmission electron microscopy (TEM) image reveals that there was 3 and 4 fold increase in the number of either sick (e.g. missing cristae structure) or broken (e.g. ruptured outer membrane structure) mitochondria in BAT collected from mice in 5 and 10 mg/kg arsenite-administered groups, respectively (Fig. 5E). Total BAT mass was significantly reduced in the group of 10 mg/kg arsenite administration (Fig. S3) due to the decrease in adipogenesis and LD droplet size and mitochondrial biogenesis.

Arsenite blocks autophagy activity through Sestrin2 and ULK1 inhibition *in vivo*. It was reported that short term treatment or exposure of arsenite increases reactive oxygen species (ROS) level and induces autophagy as a defense mechanism in human uro-epithelial cells⁴⁶. To investigate the effect of arsenite treatment on autophagy activity in BAT, we measured mRNA expression of essential autophagy genes (e.g., ULK1, Atg5, Atg7, and LC3B), stress-inducible protein Sestrin2, and autophagy receptor p62 under our experimental conditions. Sestrin2, ULK1, and p62 were significantly downregulated by arsenite (10 mg/kg BW of mice) (Fig. 6A) suggesting that arsenite may inhibit autophagy by downregulating genes involved in ULK1 induction as well as p62 receptor association with autophagosome. Sestrin2 inhibits mTORC1 through AMPK activation^{47,48}. Therefore, arsenite may inhibit gene expression of Sestrin2 to lead to mTORC1 activation through AMPK inhibition and subsequent autophagy inhibition. Although our immunoblotting data displayed a significance decrease in Sestrin2 and ULK1 expression levels in response to arsenite administration (10 mg/kg), there was no significant difference in both phosphorylation of S6K (a mTORC1 target) at Thr 389 and phosphorylation of ACC (an AMPK target) at Ser 79 (Fig. 6B). These data collectively suggest that the autophagy inhibition by arsenite is mainly attributed to the inhibition of Sestrin2 and ULK1 expression but not through direct mTORC1 or AMPK regulation. While arsenite may directly inhibit autophagosome maturation by inhibiting p62, there was no significant effect of arsenite on the expression of genes involved in the Atg5-, Atg7-, or LC3B- dependent autophagosome conjugation system (Fig. 6C).

Discussion

Increased consumption of high carbohydrate and fat containing food and westernized diet would have been a serious concern correlated with the increased rate of morbidity due to metabolic diseases such as obesity, diabetes, cardiovascular diseases, and cancer. Particularly combined with the exposure to harmful environmental pollutants and genotoxic agents in the food, water and air, it would have been major attention in combating against metabolic diseases in the modern society^{19,49}. United States environmental protection agency (EPA) classified arsenic as a Group 1A carcinogen. Over decades, majority of studies have focused on arsenic carcinogenesis in skin, lung, liver, and urinary bladder and the increased level of oxidative stress, mitochondria DNA damage, mitochondrial biogenesis, and mutation in arsenic sensitive oncogenes were believed to be major contributing factors in human⁵⁰. Unlike arsenic carcinogenesis studies, the studies on the effect of arsenic on the adipose tissue metabolism, mitochondrial function in obesity were very limited albeit the positive correlation between arsenite exposure and diabetes mellitus in Michigan residing human studies²⁵, and population studies in high arsenic areas ($\geq 150 \mu\text{g/L}$ drinking water) of Taiwan and Bangladesh⁵¹, and the molecular mechanism underlying the arsenic-induced metabolic disorders is still remained unclear.

Other arsenic research groups reported that acute high dose of arsenic ($>500 \text{ nM}$) increases ROS and subsequently upregulates antioxidant genes such as heme oxygenase and Nrf2 to protect cells from mitochondria damage and oxidative DNA damage⁵². However, low dose of arsenic ($<500 \text{ nM}$) upto 24 hrs treatment decreases ROS by inducing antioxidant genes⁵³. Furthermore, low dose of arsenic promotes cell proliferation by increasing mitochondrial biogenesis in skin cancer cells⁵⁴. It is still debatable but generally ROS-mediated cell damage and apoptosis would be considered as mechanism underlying arsenic-induced toxicity. Our data suggest that upto $10 \mu\text{M}$ of arsenite treatment did not affect the cell survival without apoptosis induction, so we investigated the effect of arsenite treatment during the course of brown adipocyte differentiation. Arsenite treatment suppressed differentiation and inhibited mitochondrial biogenesis of brown adipocytes in a dose dependent manner. This data was consistent with the inhibition of white adipocyte differentiation in previous studies^{29,30}. However, we observed 7.9 times more accumulation BAT compared to eWAT in 10 mg/kg administration of arsenite in mice. This data would suggest that arsenite-associated obesity is not only affected by inhibition of WAT function and is further aggravated by the malfunction of BAT *in vivo*. It needs further investigation why the arsenic is much heavily accumulated in BAT among adipose tissues in mice. It is possible that arsenic directly bind to the promoters of genes involved in the mitochondrial biogenesis or blocking mitochondrial turnover through inhibiting autophagy gene expression or autophagy protein activity by direct binding. Our group and others would investigate the individual arsenic specific target genes and its inhibition mechanism as further studies. High level of accumulation of arsenic prevent normal cell differentiation of adipose tissues and cause the imbalance in fat metabolism and mitochondrial functions, which can contribute to the development of metabolic disorders such as obesity and diabetes. ACC gene expression essential for lipid biogenesis was also suppressed in arsenite-administered mice group. Consistently, we have observed decrease in the lipid droplet content in BAT upon arsenite administration. Another notable result is that arsenite treatment suppresses UCP1 gene expression in the mitochondria, which are essential for thermogenic function of brown fat to dissipate energy as a heat⁵⁵. In live mice, we observed similar result while total food and water intake, oxygen consumption and RER were not changed. It is possible that there would be compensation mechanism from other tissues protecting mice since oxygen consumption and RER are vital signs essential for survival. Transgenic overexpression of mitochondrial uncoupling protein UCP1-3 in skin of mice showed strong resistance to chemically induced carcinogenesis, suggesting that inhibition of mitochondrial respiration through enhancing mitochondrial uncoupling would be a therapeutic target against arsenic-induced cancer⁵⁶. In the same context, UCP1 overexpression or UCP1 enhancing drugs would be a potential treatment to protect adipose tissues from arsenic-induced metabolic disorders. It is plausible that proper dose of arsenic chelating agents such as BAL, DMPS, and DMSA⁵⁷ or overexpressing arsenic-sequestering proteins such as Hexokinase-2 (HK2)⁵⁸ in BAT would be beneficial in improving lipid metabolism, mitochondrial function and thermogenesis, which contribute on the prevention or treatment of arsenic-induced metabolic disorders.

Short term treatment upto 48 hrs or acute exposure of arsenite induces autophagy evidenced by increasing lipidated form of LC3B (LC3B-II) and decreasing level of p62 autophagy receptor in cardiac cells, neuronal cells, and cancer cells⁵⁹⁻⁶¹. Arsenite-induced ROS in short term treatment have been suggested as a main cause to induced autophagy activity⁶². However, in recent studies using NIH3T3 fibroblasts, 4 hrs of short term treatment of arsenite activates Nrf2 pathway through autophagy inhibition⁶³. Indeed, in our autophagy studies using HIB1B brown adipocytes, we observed increased level of LC3B-II accumulation along with the accumulation of p62 by arsenite, which support the inhibition of autophagy pathway. Treatment of autophagy blocker, bafilomycin A1 also completely suppress the genes of brown adipogenesis, which also support the inhibition of brown adipocyte differentiation via autophagy inhibition by arsenite. It has been reported by several independent groups that a loss of essential autophagy genes such as Atg5 and Atg7 leads to the formation of p62-positive aggregates and accumulation of ubiquitinated protein inclusion body and Mallory bodies in the liver⁶⁴⁻⁶⁶. Autophagy has two LC3B or Atg8 conjugations systems, Atg5-Atg12⁶⁷ and Atg4-Atg7-Atg3^{68,69}. However, our data showed that arsenite mediated autophagy inhibition in BAT is independent of Atg5 and Atg7 ($P < 0.06$). Rather, Sestrin2, ULK1 and p62 inhibition by arsenite accumulation is the underlying mechanism of autophagy inhibition in BAT. Recently, Gao *et al.* reported that arsenite treatment upto $10 \mu\text{M}$ for short term 24 hrs blocks autophagy flux through LncRNA UCA1 mediated activation of mTORC1/S6K pathway in human hepatocytes⁷⁰. However, in our studies, arsenite treatment through oral gavage over longer term 9 days in mice suppressed Sestrin2 and ULK1 gene expressions but not significantly inhibiting AMPK and activating mTORC1. Ro *et al.* previously reported that Sestrin2 can directly bind with ULK1 and activate autophagy induction possibly independently from mTORC1 and AMPK⁷¹. Longer arsenite exposure would directly regulates gene expression levels of Sestrin2 and ULK1 to inhibit autophagy. Differently from cell culture model, there might be a compensation mechanism that maintains mTORC1 or AMPK activity under arsenite-induced toxicity in mammals. Our TEM image data also suggested that inhibition of autophagy activity in arsenite treatment groups

may contribute on the accumulation of damaged mitochondria in BAT. Autophagy inhibition by arsenite exposure would lead to irreversible apoptotic cell death which we observed in the reduction of total BAT mass including both mitochondria and lipid mass by arsenite. In this regard, autophagy enhancing drugs such as metformin, torins and resveratrol⁷² or the overexpression of autophagy induction proteins such as Sestrin2 and ULK1 would be protective mechanism against deregulation or loss of BAT functions affected by arsenic-induced toxicity. While our group is preparing the manuscript, two recent papers came out on publication. Consistent with our data suggesting the autophagy inhibition by arsenite, Dodson *et al.* from Dr. Zhang's group treated As (III) concentrations ranging 0.5 to 5 μM [37.5 to 375 ppb] in NIH 3T3 fibroblasts upto 48 hrs and observed that arsenic inhibits SNARE complex formation by enhancing O-GlcNAcylation of SNAP29 and drives autophagy dysfunction⁷³. However, in another arsenic research group suggested that arsenic at 50 ppm (equivalent of 50,000 ppb or 667 μM) in drinking water administration in NMRI mice under 20 weeks of HFD actually increased both macroautophagy and Chaperon-mediated autophagy (CMA) in liver tissues⁷⁴. Since the macroautophagy response is more rapid and the CMA is activated when macroautophagy is inhibited or defective under prolonged nutritional stress^{75–77}, the upregulation of gene expression levels of both macroautophagy and CMA genes would be a compensation effect of serious macroautophagy or CMA defect and possible non-apoptotic cell death in liver. From these recent publications, we speculate that the arsenic effect on autophagy function is highly debatable depending on arsenic concentrations, time, tissue types, and mice species. Therefore, our study has proposed a unique mechanism and is an independent research from liver studies regarding the long term arsenic effect on BAT function and autophagy.

In conclusion, we propose a model where arsenite exposure consistently suppresses the brown adipocyte differentiation, mitochondrial biogenesis and function, thermogenesis, and autophagy function, which would have harmful effect on metabolic balance in human body and leads to metabolic disorders. Our study supports the previous human studies performed in US and other developing countries in the world that have higher concentration of arsenite contamination in water and soil would develop higher chances of development of metabolic disorders such as obesity and diabetes^{23–25}. We believe that our study provides new clues on the connections between arsenite exposure and metabolic disorders by highlighting the major metabolic functions of BAT, which seemingly has higher accumulation of arsenic in our body. Balancing the BAT differentiation, mitochondrial integrity, thermogenesis, and autophagy activity would be novel protective mechanisms against arsenic-induced toxicity and metabolic disorders.

Methods

Reagents and antibodies. Dulbecco's modified Eagle's medium (DMEM) was purchased from Invitrogen (San Diego, CA). Fetal bovine serum (FBS), 3-isobutyl-L-methylxanthine, T3, dexamethasone, insulin, indomethacin, and Oil Red O were purchased from Sigma-Aldrich (St. Louis, MO). MTT cell growth assay kit was purchased from Sigma-Aldrich (St. Louis, MO). Primary antibodies against PPAR γ , phospho-AMPK (T172), phospho-ULK1 (Ser555), ULK1, phospho-ACC (Ser79), ACC, and S6K were purchased from Cell Signaling Technology (Danvers, MA). Tubulin and Actin antibodies was purchased from Developmental Studies Hybridoma Bank (Iowa City, IA). PGC1 α , phospho-S6K (Thr389), and AMPK antibodies were purchased from Santa Cruz Biotechnology (Dallas, TX) and UCP1 antibody was purchased from Alpha Diagnostic (San Antonio, TX). Sodium arsenite (NaAsO₂) was obtained from Sigma-Aldrich (St. Louis, MO) and a stock solution was prepared at a final concentration of 100 mM and was diluted for a working concentration in water (ddH₂O).

Brown preadipocyte culture and adipocyte differentiation. Immortalized HIB1B murine brown preadipocyte cell line, generated from the interscapular brown fat of C57BL/6 mice, is a gift from Dr. Johannes Klein (University of Lubeck, Lubeck, Germany)⁷⁸. Brown preadipocytes were maintained in DMEM supplemented with 20% FBS at 37 °C humidified atmosphere of 5% CO₂ in air. The differentiation of brown preadipocytes was as previously described⁷⁹. Briefly, cells were plated and grown in DMEM supplemented with 20% FBS until confluency (designed as D0). The cells were then changed into DMEM supplemented with 20% FBS, 1 nM T3, 20 nM insulin, 0.125 mM indomethacin, 5 μM dexamethasone, and 0.5 mM 3-isobutyl-L-methylxanthine for 24 hrs, followed by DMEM supplemented with 20% FBS, 1 nM T3, and 20 nM insulin, replenished every two days until the cells were fully differentiated at Day 6 (D6). Sodium arsenite was added to the media at D0 and replaced with each change of the media during the process. All experiments were performed in room temperature (23 °C) unless it is specifically indicated as in cold temperature (4 °C).

Oil red O staining and quantification. Fully differentiated brown adipocytes were fixed with 10% formalin overnight, and the lipid droplets were stained with Oil Red O and quantified by absorbance at 500 nm in a spectrophotometer.

Immunoblotting analysis. Total cell lysates were prepared in RIPA buffer (50 mM Tris-Cl pH 7.4, 150 mM NaCl, 1% sodium deoxycholate, 1% NP-40; 0.1% SDS) or cell lysis buffer (20 mM Tris-Cl pH 7.5, 150 mM NaCl, 1 mM EDTA, 1 mM EGTA, 2.5 mM sodium pyrophosphate, 1 mM β -glycerophosphate, 1 mM Na₃VO₄, 1% Triton-X-100) containing protease inhibitor cocktail (Roche) and phosphatase inhibitor (Sigma) and protein concentrations were determined by BCA assay kit (Thermo Scientific, Waltham, MA). Thirty micrograms of total cell lysates were subjected to 4–20% SDS-PAGE and transferred to polyvinylidene difluoride membrane. The membrane was blocked in 20 mM Tris-HCl, 137 mM NaCl, and 0.2% Tween 20 (pH 7.6) containing 5% nonfat milk. The membrane was immunoblotted with primary antibodies at 4 °C overnight followed by secondary antibody conjugated with horseradish peroxidase (Bio-Rad, Hercules, CA) for 1 hr. The membrane was exposed on X-ray film using ECL Western blot detection reagents (Pierce Biotechnology, Rockford, IL) or digitally captured using Odyssey blot imager (LI-COR, Lincoln, NE). Raw uncropped images with molecular size marker were displayed in the supplementary section (Figs S4–S9). Immunoblot band density was measured by ImageJ program (National Institute of Health) and normalized by the intensity of loading control (Tubulin or Actin) as indicated.

RNA preparation and quantitative real-time PCR analysis. Total RNA was prepared using TRIzol (Invitrogen). Total RNA abundance was quantified using a NanoDrop Spectrophotometer (NanoDrop Technologies, Wilmington, DE). Reverse transcription was carried out using High Capacity cDNA Reverse Transcription kit (Thermo Scientific, Pittsburgh, PA) according to the manufacturer's instructions. mRNA expression of target genes and housekeeping gene (Table S1) were measured quantitatively using SoAdvanced Universal SYBR Green Supermix (Bio-Rad, Hercules, CA). PCR reactions were run in 96-well plate using MyiQ Real-Time PCR Detection System (Bio-Rad, Hercules, CA). Cycle conditions were 95 °C for 5 min, then 40 cycles of 95 °C for 15 sec/60 °C for 30 sec. Relative gene expression was calculated using the $2^{-\Delta\Delta Ct}$ method, which normalizes against loading control β -actin.

Analysis of mitochondrial content by MitoTracker staining. Mitochondria were labeled using the mitochondria-specific dye MitoTracker Red (Invitrogen, Carlsbad, CA) according to manufacturer's protocol. Briefly, the differentiated brown adipocytes were washed and incubated with 100 nM MitoTracker Red for 30 min at 37 °C. Image was taken with Leica DMI4000B fluorescence microscope (Leica Microsystems, Wetzlar, Germany). The fluorescence intensity was measured with Synergy H1 Hybrid Multi-Mode Reader (BioTek Instruments, Winooski, VT). Relative fluorescence intensity is the fold of the mean fluorescence intensity of the controls.

Mitochondrial respiration measurements. Five thousand of brown preadipocytes were seeded in gelatin-coated 24-well XF assay plates in the 10% FBS containing DMEM and differentiated in the presence or absence of arsenite for 6 days. Differentiated brown adipocytes were rinsed 3 times, changed to 500 μ L of XF assay buffer, and equilibrated at non-CO₂ incubator at 37 °C for 1 hr. The cells subjected to real-time measurements of oxygen consumption rate (OCR) using XF24 Extracellular Flux Analyzer (Agilent Seahorse, Santa Clara, CA) as previously reported^{45,55}. For mitochondrial stress tests, mitochondrial complex inhibitors were injected to all of the following treatments sequentially in the following order: oligomycin (1 μ M), carbonyl cyanide-p-trifluoromethoxyphenylhydrazone (FCCP; 0.75 μ M), antimycin A/rotenone (2.5 μ M each), and 3 readings were taken after each injection. OCR was automatically recorded by XF24 software v2.3 provided by the manufacturer. Calculations of proton leak, coupling efficiency, maximal respiration, and ATP production were performed according to the manufacturer's instructions.

Animal handling. Housing and use of mice in the study were performed in compliance with the National Institute of Health (NIH) Principles for the Use of Animals, the American Veterinary Medical Association (AVMA) Guidelines, and the Public Health Service Policy on Humane Care and Use of Laboratory Animals awarded by University of Nebraska-Lincoln (Animal Welfare Assurance Number: A3459-01). Animal care and experimental procedures were approved by the institutional Animal Care and Use Committee (IACUC Approval Number: 1310 and 1527). Seven-week-old male C57BL/6J mice (Stock No. 000664, 21–23 g) were purchased from Jackson Laboratory (Bar Harbor, ME)^{80–82}. They were maintained for a week to acclimate to their new environment before performing the experiments. Animals were housed in a group of three or four mice per cage (501 cm² floor area; Tecniplast, Italy) with Tek-Fresh bedding (Harlan Teklad, Madison, WI) under a 12-h light/dark cycle from 06:00 to 18:00. They were fed the standard chow diet (Catalog #2016C, Envigo, Madison, WI) contains 16% protein and 4% fat to cover 12% of total kcal and sterilized drinking water *ad libitum*. Mice were euthanized according to IACUC protocol after the completion of experiments.

Oral administration of arsenite in mice and tissue collection. Sodium arsenite stock solution at 200 mg/mL was prepared by dissolving in distilled regular water. The arsenite stock solution was aliquoted and stored in –80 °C until use. The arsenite was orally administered to mice at doses of 5 and 10 mg/kg after diluting the arsenite stock solution with distilled water ($n = 6$ per group). A control group was given regular water at a dosing volume of 5 mL/kg which was comparable to the volume of arsenite administered groups^{83,84}. The arsenite was administered to mice once a day for 9 days (Day 1 to 9)^{85–88}. In the case of *in vivo*, we wanted to quantify the accumulated amount of arsenic in mice adipose tissues. The major source of arsenic exposure is drinking water and food. The exposure ordinarily occurs chronically. To ensure all mice ingested equal arsenic, we decided to administer arsenite to mice orally by gavage rather than including it in drinking water and food. The arsenic dose and treatment period were determined by tissue distribution and toxicity in consideration of the previous reports^{83–88}. To check the levels of mRNA in BAT and to compare the change of them under different temperature, mice were divided into room temperature (RT, 23 °C) or cold temperature (4 °C). The mice under cold condition were transferred to cold room (4 °C) on Day 9 for 24 hrs. The body weight of mice was measured from Day 0 to 10. The epididymal white adipose tissue (eWAT), inguinal white adipose tissue (ingWAT), and interscapular brown adipose tissue (BAT) of all mice were collected on Day 10 under anesthesia with isoflurane and CO₂. All samples were measured individually and stored at –80 °C until use. All experiments were performed in RT unless it is specifically indicated as in cold temperature.

Quantification of arsenic content in adipose tissue. Arsenic analysis was performed using an Inductively Coupled Plasma Mass Spectrometry (ICP-MS) 7500cx series (Agilent Technologies, Santa Clara, CA) and an ESI SC-4 high-throughput auto sampler (Elemental Scientific, Omaha, NE). All mice adipose tissue (eWAT, ingWAT or BAT) samples were homogenized in PBS containing Complete Protease Inhibitor Cocktail (Roche, Basel, Switzerland). To normalize the lysate samples, the amount of protein in each lysate was measured using the Bradford Protein Assay (Bio-Rad, Hercules, CA). The adipose tissue samples were suspended in 200 μ L of nitric acid with 50 μ g/L of gallium as an internal standard. For complete digestion of fat, WAT samples were incubated overnight with 200 μ L of nitric acid and internal standard followed by adding 200 μ L of H₂O₂ and incubated for 15 hrs. The suspended adipose tissue samples were diluted 1–20 times into the auto sampler plate to analysis the arsenic content. Each sample was analyzed 3 times. The carrier solution was 1.5% nitric acid at a flow rate of 70 mL/min and the injection volume was 70 μ L.

Transmission electron microscopy (TEM) imaging. Brown adipocyte tissue was extracted from mice and reduced to three 1-mm pieces. Samples were fixed with 2.5% glutaraldehyde in 0.1 M cacodylate buffer (pH 7.4) for 1 hr at RT and then overnight at 4 °C. Samples were then post-fixed with 1% osmium tetroxide for 1 hr at RT. Fixed tissues were dehydrated through a graduated ethanol series and embedded in Spurr (Electron Microscopic Sciences, Fort Washington, PA). Ultrathin sections (~80 nm) were stained with uranyl acetate and lead citrate and observed under a transmission electron microscope (Hitachi H7500-I). A series of ultrastructural images were collected with a bottom-mount digital camera.

Measurement of food and water intake and mitochondrial respiratory rate. The food and water intakes and respiratory rate of mice were measured using metabolic cages (TSE systems, Chesterfield, MO) during arsenite treatment period ($n = 4$ per group). The metabolic profiles were investigated by a computer controlled monitoring systems of metabolic cages as previously reported⁴⁵. Mice were housed in groups before they were in the metabolic cages (Day 0 to 2) and then acclimated in metabolic cages, one mouse per cage, for a day (Day 3). They also were in the metabolic cages alone while the food and water intakes and respiratory rate were measured for 5 days (Day 4 to 9).

Histology. A portion of the collected BAT samples was prepared for histology. These tissues were placed in cassettes and fixed in 10% formalin. All tissues were processed on a Leica Peloris tissue processor (Leica Biosystems, Wetzlar, Germany). The prepared sections (4 microns) were stained with haematoxylin and eosin (StatLab, McKinney, TX). Tissue slides were evaluated by light microscopy at 400X magnification. Six microphotographs per mouse were obtained. The lipid-droplet diameter of BAT tissues was calculated from the mean of ten values per microphotograph.

Statistical analysis. All data are presented as mean \pm SEM. Measurements were performed at least in triplicates. Statistical analysis was performed using SPSS 25 (IBM Corporation, Armonk, NY). One-way ANOVA was performed by Tukey's multiple comparison test to determine the differences of group mean among control and two treatment groups. The level of significance was set at $*P < 0.05$ or $**P < 0.01$.

References

- Shigetoh, Y. *et al.* Higher heart rate may predispose to obesity and diabetes mellitus: 20-year prospective study in a general population. *Am J Hypertens* **22**, 151–155, <https://doi.org/10.1038/ajh.2008.331> (2009).
- Re, R. N. Obesity-related hypertension. *Ochsner J* **9**, 133–136 (2009).
- Apovian, C. M. & Gokce, N. Obesity and cardiovascular disease. *Circulation* **125**, 1178–1182, <https://doi.org/10.1161/CIRCULATIONAHA.111.022541> (2012).
- Basen-Engquist, K. & Chang, M. Obesity and cancer risk: recent review and evidence. *Curr Oncol Rep* **13**, 71–76, <https://doi.org/10.1007/s11912-010-0139-7> (2011).
- Lee, Y. H., Mottillo, E. P. & Granneman, J. G. Adipose tissue plasticity from WAT to BAT and in between. *Biochim Biophys Acta* **1842**, 358–369, <https://doi.org/10.1016/j.bbdis.2013.05.011> (2014).
- McMillan, A. C. & White, M. D. Induction of thermogenesis in brown and beige adipose tissues: molecular markers, mild cold exposure and novel therapies. *Curr Opin Endocrinol Diabetes Obes* **22**, 347–352, <https://doi.org/10.1097/MED.000000000000191> (2015).
- Saelly, C. H., Geiger, K. & Drexel, H. Brown versus white adipose tissue: a mini-review. *Gerontology* **58**, 15–23, <https://doi.org/10.1159/000321319> (2012).
- van Marken Lichtenbelt, W. D. & Schrauwen, P. Implications of nonshivering thermogenesis for energy balance regulation in humans. *Am J Physiol Regul Integr Comp Physiol* **301**, R285–296, <https://doi.org/10.1152/ajpregu.00652.2010> (2011).
- Virtanen, K. A., van Marken Lichtenbelt, W. D. & Nuutila, P. Brown adipose tissue functions in humans. *Biochim Biophys Acta* **1831**, 1004–1008, <https://doi.org/10.1016/j.bbali.2012.12.011> (2013).
- Azzu, V. & Brand, M. D. The on-off switches of the mitochondrial uncoupling proteins. *Trends Biochem Sci* **35**, 298–307, <https://doi.org/10.1016/j.tibs.2009.11.001> (2010).
- Brondani, L. A. *et al.* The role of the uncoupling protein 1 (UCP1) on the development of obesity and type 2 diabetes mellitus. *Arq Bras Endocrinol Metabol* **56**, 215–225 (2012).
- Cohen, P. *et al.* Ablation of PRDM16 and beige adipose causes metabolic dysfunction and a subcutaneous to visceral fat switch. *Cell* **156**, 304–316, <https://doi.org/10.1016/j.cell.2013.12.021> (2014).
- Harms, M. & Seale, P. Brown and beige fat: development, function and therapeutic potential. *Nat Med* **19**, 1252–1263, <https://doi.org/10.1038/nm.3361> (2013).
- Lanthier, N. & Leclercq, I. A. Adipose tissues as endocrine target organs. *Best Pract Res Clin Gastroenterol* **28**, 545–558, <https://doi.org/10.1016/j.bpg.2014.07.002> (2014).
- Cypess, A. M. *et al.* Identification and importance of brown adipose tissue in adult humans. *N Engl J Med* **360**, 1509–1517, <https://doi.org/10.1056/NEJMoa0810780> (2009).
- van Marken Lichtenbelt, W. D. *et al.* Cold-activated brown adipose tissue in healthy men. *N Engl J Med* **360**, 1500–1508, <https://doi.org/10.1056/NEJMoa0808718> (2009).
- Holstila, M. *et al.* Measurement of brown adipose tissue mass using a novel dual-echo magnetic resonance imaging approach: a validation study. *Metabolism* **62**, 1189–1198, <https://doi.org/10.1016/j.metabol.2013.03.002> (2013).
- Park, J. W. *et al.* ¹⁸F-FDG PET/CT monitoring of beta3 agonist-stimulated brown adipocyte recruitment in white adipose tissue. *J Nucl Med* **56**, 153–158, <https://doi.org/10.2967/jnumed.114.147603> (2015).
- Hughes, M. F., Beck, B. D., Chen, Y., Lewis, A. S. & Thomas, D. J. Arsenic exposure and toxicology: a historical perspective. *Toxicol Sci* **123**, 305–332, <https://doi.org/10.1093/toxsci/kfr184> (2011).
- Kleiman, N. J., Quinn, A. M., Fields, K. G., Slavkovich, V. & Graziano, J. H. Arsenite accumulation in the mouse eye. *J Toxicol Environ Health A* **79**, 339–341, <https://doi.org/10.1080/15287394.2016.1151392> (2016).
- Li, Q. *et al.* The preferential accumulation of heavy metals in different tissues following frequent respiratory exposure to PM 2.5 in rats. *Sci Rep* **5**, 16936, <https://doi.org/10.1038/srep16936> (2015).
- Perry, M. R., Wyllie, S., Raab, A., Feldmann, J. & Fairlamb, A. H. Chronic exposure to arsenic in drinking water can lead to resistance to antimonial drugs in a mouse model of visceral leishmaniasis. *Proc Natl Acad Sci USA* **110**, 19932–19937, <https://doi.org/10.1073/pnas.1311535110> (2013).
- D'Ipolliti, D. *et al.* Arsenic in Drinking Water and Mortality for Cancer and Chronic Diseases in Central Italy, 1990–2010. *PLoS One* **10**, e0138182, <https://doi.org/10.1371/journal.pone.0138182> (2015).
- Brauner, E. V. *et al.* Long-term exposure to low-level arsenic in drinking water and diabetes incidence: a prospective study of the diet, cancer and health cohort. *Environ Health Perspect* **122**, 1059–1065, <https://doi.org/10.1289/ehp.1408198> (2014).

25. Meliker, J. R., Wahl, R. L., Cameron, L. L. & Nriagu, J. O. Arsenic in drinking water and cerebrovascular disease, diabetes mellitus, and kidney disease in Michigan: a standardized mortality ratio analysis. *Environ Health* **6**, 4, <https://doi.org/10.1186/1476-069X-6-4> (2007).
26. Renu, K. *et al.* Role of arsenic exposure in adipose tissue dysfunction and its possible implication in diabetes pathophysiology. *Toxicol Lett* **284**, 86–95, <https://doi.org/10.1016/j.toxlet.2017.11.032> (2018).
27. Ceja-Galicia, Z. A. *et al.* Effects of arsenic on adipocyte metabolism: Is arsenic an obesogen? *Mol Cell Endocrinol* **452**, 25–32, <https://doi.org/10.1016/j.mce.2017.05.008> (2017).
28. Klei, L. R., Garciafigueroa, D. Y. & Barchowsky, A. Arsenic activates endothelin-1 Gi protein-coupled receptor signaling to inhibit stem cell differentiation in adipogenesis. *Toxicol Sci* **131**, 512–520, <https://doi.org/10.1093/toxsci/kfs323> (2013).
29. Wang, Z. X. *et al.* The role of Akt on arsenic trioxide suppression of 3T3-L1 preadipocyte differentiation. *Cell Res* **15**, 379–386, <https://doi.org/10.1038/sj.cr.7290305> (2005).
30. Trouba, K. J., Wauson, E. M. & Vorce, R. L. Sodium arsenite inhibits terminal differentiation of murine C3H 10T1/2 preadipocytes. *Toxicol Appl Pharmacol* **168**, 25–35, <https://doi.org/10.1006/taap.2000.9012> (2000).
31. Garciafigueroa, D. Y., Klei, L. R., Ambrosio, F. & Barchowsky, A. Arsenic-stimulated lipolysis and adipose remodeling is mediated by G-protein-coupled receptors. *Toxicol Sci* **134**, 335–344, <https://doi.org/10.1093/toxsci/kft108> (2013).
32. Galluzzi, L. *et al.* Molecular definitions of autophagy and related processes. *EMBO J* **36**, 1811–1836, <https://doi.org/10.15252/embj.201796697> (2017).
33. Egan, D. F. *et al.* Phosphorylation of ULK1 (hATG1) by AMP-activated protein kinase connects energy sensing to mitophagy. *Science* **331**, 456–461, <https://doi.org/10.1126/science.1196371> (2011).
34. Kim, J., Kundu, M., Viollet, B. & Guan, K. L. AMPK and mTOR regulate autophagy through direct phosphorylation of Ulk1. *Nat Cell Biol* **13**, 132–141, <https://doi.org/10.1038/ncb2152> (2011).
35. Jung, C. H. *et al.* ULK-Atg13-FIP200 complexes mediate mTOR signaling to the autophagy machinery. *Mol Biol Cell* **20**, 1992–2003, <https://doi.org/10.1091/mbc.E08-12-1249> (2009).
36. Jung, C. H., Ro, S. H., Cao, J., Otto, N. M. & Kim, D. H. mTOR regulation of autophagy. *FEBS Lett* **584**, 1287–1295, <https://doi.org/10.1016/j.febslet.2010.01.017> (2010).
37. Katsuragi, Y., Ichimura, Y. & Komatsu, M. p62/SQSTM1 functions as a signaling hub and an autophagy adaptor. *FEBS J* **282**, 4672–4678, <https://doi.org/10.1111/febs.13540> (2015).
38. Dikic, I. & Elazar, Z. Mechanism and medical implications of mammalian autophagy. *Nat Rev Mol Cell Biol*, <https://doi.org/10.1038/s41580-018-0003-4> (2018).
39. Ahmed, M. *et al.* Systematic characterization of autophagy-related genes during the adipocyte differentiation using public-access data. *Oncotarget* **9**, 15526–15541, <https://doi.org/10.18632/oncotarget.24506> (2018).
40. Baerga, R., Zhang, Y., Chen, P. H., Goldman, S. & Jin, S. Targeted deletion of autophagy-related 5 (atg5) impairs adipogenesis in a cellular model and in mice. *Autophagy* **5**, 1118–1130 (2009).
41. Zhang, Y. *et al.* Adipose-specific deletion of autophagy-related gene 7 (atg7) in mice reveals a role in adipogenesis. *Proc Natl Acad Sci USA* **106**, 19860–19865, <https://doi.org/10.1073/pnas.0906048106> (2009).
42. Ro, S. H. *et al.* Distinct functions of Ulk1 and Ulk2 in the regulation of lipid metabolism in adipocytes. *Autophagy* **9**, 2103–2114, <https://doi.org/10.4161/auto.26563> (2013).
43. Dadson, P. *et al.* Brown adipose tissue lipid metabolism in morbid obesity: Effect of bariatric surgery-induced weight loss. *Diabetes Obes Metab* **20**, 1280–1288, <https://doi.org/10.1111/dom.13233> (2018).
44. Rui, L. B. and Beige Adipose Tissues in Health and Disease. *Compr Physiol* **7**, 1281–1306, <https://doi.org/10.1002/cphy.c170001> (2017).
45. Ro, S. H. *et al.* Sestrin2 inhibits uncoupling protein 1 expression through suppressing reactive oxygen species. *Proc Natl Acad Sci USA* **111**, 7849–7854, <https://doi.org/10.1073/pnas.1401787111> (2014).
46. Huang, Y. C., Yu, H. S. & Chai, C. Y. Roles of oxidative stress and the ERK1/2, PTEN and p70S6K signaling pathways in arsenite-induced autophagy. *Toxicol Lett* **239**, 172–181, <https://doi.org/10.1016/j.toxlet.2015.09.022> (2015).
47. Budanov, A. V. & Karin, M. p53 target genes sestrin1 and sestrin2 connect genotoxic stress and mTOR signaling. *Cell* **134**, 451–460, <https://doi.org/10.1016/j.cell.2008.06.028> (2008).
48. Lee, J. H. *et al.* Maintenance of metabolic homeostasis by Sestrin2 and Sestrin3. *Cell Metab* **16**, 311–321, <https://doi.org/10.1016/j.cmet.2012.08.004> (2012).
49. Yu, H. S., Lee, C. H., Jee, S. H., Ho, C. K. & Guo, Y. L. Environmental and occupational skin diseases in Taiwan. *J Dermatol* **28**, 628–631 (2001).
50. Lee, C. H. & Yu, H. S. Role of mitochondria, ROS, and DNA damage in arsenic induced carcinogenesis. *Front Biosci (Schol Ed)* **8**, 312–320 (2016).
51. Maull, E. A. *et al.* Evaluation of the association between arsenic and diabetes: a National Toxicology Program workshop review. *Environ Health Perspect* **120**, 1658–1670, <https://doi.org/10.1289/ehp.1104579> (2012).
52. Huerta-Olvera, S. G. *et al.* Alpha-lipoic acid regulates heme oxygenase gene expression and nuclear Nrf2 activation as a mechanism of protection against arsenic exposure in HepG2 cells. *Environ Toxicol Pharmacol* **29**, 144–149, <https://doi.org/10.1016/j.etap.2009.12.004> (2010).
53. Snow, E. T., Sykora, P., Durham, T. R. & Klein, C. B. Arsenic, mode of action at biologically plausible low doses: what are the implications for low dose cancer risk? *Toxicol Appl Pharmacol* **207**, 557–564, <https://doi.org/10.1016/j.taap.2005.01.048> (2005).
54. Lee, C. H. *et al.* Aberrant cell proliferation by enhanced mitochondrial biogenesis via mtTFA in arsenical skin cancers. *Am J Pathol* **178**, 2066–2076, <https://doi.org/10.1016/j.ajpath.2011.01.056> (2011).
55. Ro, S. H., Sempke, I., Ho, A., Park, H. W. & Lee, J. H. Sestrin2, a Regulator of Thermogenesis and Mitohormesis in Brown Adipose Tissue. *Front Endocrinol (Lausanne)* **6**, 114, <https://doi.org/10.3389/fendo.2015.00114> (2015).
56. Lago, C. U. *et al.* Mitochondrial respiratory uncoupling promotes keratinocyte differentiation and blocks skin carcinogenesis. *Oncogene* **31**, 4725–4731, <https://doi.org/10.1038/nc.2011.630> (2012).
57. Kosnett, M. J. The role of chelation in the treatment of arsenic and mercury poisoning. *J Med Toxicol* **9**, 347–354, <https://doi.org/10.1007/s13181-013-0344-5> (2013).
58. Zhang, H. N. *et al.* Systematic identification of arsenic-binding proteins reveals that hexokinase-2 is inhibited by arsenic. *Proc Natl Acad Sci USA* **112**, 15084–15089, <https://doi.org/10.1073/pnas.1521316112> (2015).
59. Bessho, M. *et al.* Rho-kinase inhibitor Y-27632 attenuates arsenic trioxide toxicity in H9c2 cardiomyoblastoma cells. *Cardiovasc Toxicol* **13**, 267–277, <https://doi.org/10.1007/s12012-013-9206-2> (2013).
60. Pucer, A. *et al.* Differential role of cathepsins B and L in autophagy-associated cell death induced by arsenic trioxide in U87 human glioblastoma cells. *Biol Chem* **391**, 519–531, <https://doi.org/10.1515/BC.2010.050> (2010).
61. Qi, Y. *et al.* Autophagy in arsenic carcinogenesis. *Exp Toxicol Pathol* **66**, 163–168, <https://doi.org/10.1016/j.etp.2014.01.004> (2014).
62. Azad, M. B., Chen, Y. & Gibson, S. B. Regulation of autophagy by reactive oxygen species (ROS): implications for cancer progression and treatment. *Antioxid Redox Signal* **11**, 777–790, <https://doi.org/10.1089/ARS.2008.2270> (2009).
63. Lau, A. *et al.* Arsenic inhibits autophagic flux, activating the Nrf2-Keap1 pathway in a p62-dependent manner. *Mol Cell Biol* **33**, 2436–2446, <https://doi.org/10.1128/MCB.01748-12> (2013).
64. Komatsu, M. *et al.* The selective autophagy substrate p62 activates the stress responsive transcription factor Nrf2 through inactivation of Keap1. *Nat Cell Biol* **12**, 213–223, <https://doi.org/10.1038/ncb2021> (2010).

65. Takamura, A. *et al.* Autophagy-deficient mice develop multiple liver tumors. *Genes Dev* **25**, 795–800, <https://doi.org/10.1101/gad.2016211> (2011).
66. Lahiri, P. *et al.* p62/Sequestosome-1 Is Indispensable for Maturation and Stabilization of Mallory-Denk Bodies. *PLoS One* **11**, e0161083, <https://doi.org/10.1371/journal.pone.0161083> (2016).
67. Hanada, T. *et al.* The Atg12-Atg5 conjugate has a novel E3-like activity for protein lipidation in autophagy. *J Biol Chem* **282**, 37298–37302, <https://doi.org/10.1074/jbc.C700195200> (2007).
68. Ichimura, Y. *et al.* *In vivo* and *in vitro* reconstitution of Atg8 conjugation essential for autophagy. *J Biol Chem* **279**, 40584–40592, <https://doi.org/10.1074/jbc.M405860200> (2004).
69. Nakatogawa, H., Ichimura, Y. & Ohsumi, Y. Atg8, a ubiquitin-like protein required for autophagosome formation, mediates membrane tethering and hemifusion. *Cell* **130**, 165–178, <https://doi.org/10.1016/j.cell.2007.05.021> (2007).
70. Gao, M., Li, C., Xu, M., Liu, Y. & Liu, S. LncRNA UCA1 attenuates autophagy-dependent cell death through blocking autophagic flux under arsenic stress. *Toxicol Lett* **284**, 195–204, <https://doi.org/10.1016/j.toxlet.2017.12.009> (2018).
71. Ro, S. H. *et al.* Sestrin2 promotes Unc-51-like kinase 1 mediated phosphorylation of p62/sequestosome-1. *FEBS J* **281**, 3816–3827, <https://doi.org/10.1111/febs.12905> (2014).
72. Galluzzi, L., Bravo-San Pedro, J. M., Levine, B., Green, D. R. & Kroemer, G. Pharmacological modulation of autophagy: therapeutic potential and persisting obstacles. *Nat Rev Drug Discov* **16**, 487–511, <https://doi.org/10.1038/nrd.2017.22> (2017).
73. Dodson, M. *et al.* Increased O-GlcNAcylation of SNAP29 drives arsenic-induced autophagic dysfunction. *Mol Cell Biol*, <https://doi.org/10.1128/MCB.00595-17> (2018).
74. Zeinvand-Lorestani, M. *et al.* Autophagy upregulation as a possible mechanism of arsenic induced diabetes. *Sci Rep* **8**, 11960, <https://doi.org/10.1038/s41598-018-30439-0> (2018).
75. Cuervo, A. M., Knecht, E., Terlecky, S. R. & Dice, J. F. Activation of a selective pathway of lysosomal proteolysis in rat liver by prolonged starvation. *Am J Physiol* **269**, C1200–1208, <https://doi.org/10.1152/ajpcell.1995.269.5.C1200> (1995).
76. Kiffin, R., Christian, C., Knecht, E. & Cuervo, A. M. Activation of chaperone-mediated autophagy during oxidative stress. *Mol Biol Cell* **15**, 4829–4840, <https://doi.org/10.1091/mbc.e04-06-0477> (2004).
77. Kaushik, S., Massey, A. C., Mizushima, N. & Cuervo, A. M. Constitutive activation of chaperone-mediated autophagy in cells with impaired macroautophagy. *Mol Biol Cell* **19**, 2179–2192, <https://doi.org/10.1091/mbc.E07-11-1155> (2008).
78. Klein, J., Fasshauer, M., Klein, H. H., Benito, M. & Kahn, C. R. Novel adipocyte lines from brown fat: a model system for the study of differentiation, energy metabolism, and insulin action. *Bioessays* **24**, 382–388, <https://doi.org/10.1002/bies.10058> (2002).
79. Bae, J. *et al.* Activation of pattern recognition receptors in brown adipocytes induces inflammation and suppresses uncoupling protein 1 expression and mitochondrial respiration. *Am J Physiol Cell Physiol* **306**, C918–930, <https://doi.org/10.1152/ajpcell.00249.2013> (2014).
80. Fontaine, D. A. & Davis, D. B. Attention to Background Strain Is Essential for Metabolic Research: C57BL/6 and the International Knockout Mouse Consortium. *Diabetes* **65**, 25–33, <https://doi.org/10.2337/db15-0982> (2016).
81. Drobná, Z. *et al.* Disruption of the arsenic (+3 oxidation state) methyltransferase gene in the mouse alters the phenotype for methylation of arsenic and affects distribution and retention of orally administered arsenate. *Chem Res Toxicol* **22**, 1713–1720, <https://doi.org/10.1021/tx900179r> (2009).
82. Hughes, M. F., Kenyon, E. M., Edwards, B. C., Mitchell, C. T. & Thomas, D. J. Strain-dependent disposition of inorganic arsenic in the mouse. *Toxicology* **137**, 95–108 (1999).
83. Kenyon, E. M., Del Razo, L. M. & Hughes, M. F. Tissue distribution and urinary excretion of inorganic arsenic and its methylated metabolites in mice following acute oral administration of arsenate. *Toxicol Sci* **85**, 468–475, <https://doi.org/10.1093/toxsci/kfi107> (2005).
84. Hughes, M. F., Menache, M. & Thompson, D. J. Dose-dependent disposition of sodium arsenate in mice following acute oral exposure. *Fundam Appl Toxicol* **22**, 80–89 (1994).
85. Sanchez-Pena, L. C. *et al.* Arsenic species, AS3MT amount, and AS3MT gene expression in different brain regions of mouse exposed to arsenite. *Environ Res* **110**, 428–434, <https://doi.org/10.1016/j.envres.2010.01.007> (2010).
86. Torres-Avila, M., Leal-Galicia, P., Sanchez-Pena, L. C., Del Razo, L. M. & Gonsebatt, M. E. Arsenite induces aquaglyceroporin 9 expression in murine livers. *Environ Res* **110**, 443–447, <https://doi.org/10.1016/j.envres.2009.08.009> (2010).
87. Garcia-Montalvo, E. A., Valenzuela, O. L., Sanchez-Pena, L. C., Albores, A. & Del Razo, L. M. Dose-dependent urinary phenotype of inorganic arsenic methylation in mice with a focus on trivalent methylated metabolites. *Toxicol Mech Methods* **21**, 649–655, <https://doi.org/10.3109/15376516.2011.603765> (2011).
88. Rodriguez, V. M. *et al.* Glutathione reductase inhibition and methylated arsenic distribution in Cd1 mice brain and liver. *Toxicol Sci* **84**, 157–166, <https://doi.org/10.1093/toxsci/kfi057> (2005).

Acknowledgements

We thank Drs J. Klein (University of Lubeck, Germany), P. Black, C. DiRusso, J. Lee, O. Khalimonchuk, X. Sun, J. Lim, J. Zempleni, S. Chung (University of Nebraska-Lincoln, UNL), J. Barycki, and M. Simpson (UNL and North Carolina State University) for sharing cell lines, reagents and access to lab equipment. We thank Ro lab members for technical assistance and helpful discussion. We are grateful to Dr. S. Alvarez from Proteomics and Metabolomics core, Dr. Y. Zhou from Microscopy core, Dr. B. Brodersen and staff from Veterinary Diagnostics Center, and Dr. Y. Wang and staff from Biomedical and Obesity Research Core at UNL. This research was supported by Undergraduate Creative Activities and Research Experience (UCARE) program-scholarship from the Pepsi Quasi Endowment and Union Bank & Trust to K. Mahato and C. Schaecher, University of Nebraska ARD/ORED/BIOC grants, Layman awards, Nebraska Tobacco Settlement-Biomedical research enhancement funds and Nebraska Center for the Prevention of Obesity Diseases (NPOD) seed grant from NIH (P20GM104320) to S.-H. Ro.

Author Contributions

J.B., Y.J., H.K. and S.-H.R. conceived the experiments, J.B., H.K., K.M., C.S. and E.K. performed cell culture experiments. Y.J., H.K. and I.K. performed mouse experiments. J.B., Y.J., H.K. and S.-H.R. prepared the manuscript. S.-H.R. developed and directed the research project. All authors discussed the experimental results and reviewed the manuscript.

Additional Information

Supplementary information accompanies this paper at <https://doi.org/10.1038/s41598-019-50965-9>.

Competing Interests: The authors declare no competing interests.

Publisher's note Springer Nature remains neutral with regard to jurisdictional claims in published maps and institutional affiliations.



Open Access This article is licensed under a Creative Commons Attribution 4.0 International License, which permits use, sharing, adaptation, distribution and reproduction in any medium or format, as long as you give appropriate credit to the original author(s) and the source, provide a link to the Creative Commons license, and indicate if changes were made. The images or other third party material in this article are included in the article's Creative Commons license, unless indicated otherwise in a credit line to the material. If material is not included in the article's Creative Commons license and your intended use is not permitted by statutory regulation or exceeds the permitted use, you will need to obtain permission directly from the copyright holder. To view a copy of this license, visit <http://creativecommons.org/licenses/by/4.0/>.

© The Author(s) 2019